NANO LETTERS

pubs.acs.org/NanoLett

Few-Femtosecond Plasmon Dephasing of a Single Metallic Nanostructure from Optical Response Function Reconstruction by Interferometric Frequency Resolved Optical Gating

Alexandria Anderson,[†,⊥,#] Kseniya S. Deryckx,[†,‡,⊥] Xiaoji G. Xu,[†,⊥] Günter Steinmeyer,[§,∥] and Markus B. Raschke*[,†,‡]

[†]Department of Chemistry and [‡]Department of Physics, University of Washington, Seattle, Washington 98195, [§]Max-Born-Institut für Nichtlineare Optik und Kurzzeitspektroskopie, D-12489 Berlin, Germany, and [∥]Optoelectronics Research Centre, Tampere University of Technology, 33720 Tampere, Finland

ABSTRACT The precise characterization of the ultrafast optical response of metals and metallic nanostructures has remained an experimental challenge. We probe the few-femtosecond electronic dephasing of a local surface plasmon polariton excitation using symmetry-selective second-harmonic (SH) Rayleigh scattering of a nanoscopic conical gold tip as an individual plasmonic nanostructure. The full reconstruction of the optical response function of the plasmon excitation with phase and amplitude without any model assumptions is demonstrated from the analysis of the two-dimensional spectrogram obtained by simultaneous time- and frequency-domain SH measurements, using interferometric frequency resolved optical gating. The measured dephasing time of $T_2 = 18 \pm 5$ fs indicates the plasmon damping is dominated by nonradiative decay, consistent with a Drude−Sommerfeld dielectric response for gold. Even for the nominally homogeneous localized plasmon response, deviations are observed from the ideal harmonic oscillator phase behavior, which may reflect the underlying inhomogeneous electronic response with its different scattering channels. The presented technique is generally applicable for the reconstruction of the plasmon dynamics of complex nanostructures: information that cannot be obtained by conventional dark-field scattering.

KEYWORDS Plasmon dephasing, nonlinear dynamics, FROG, nanotip

The electron dynamics of metals are governed by the interaction and scattering of electrons with other charge carriers, phonons, defects, and impurities. They therefore reflect the underlying elementary processes, for example, the optical properties, charge, and thermal transport of metals and metal nanostructures, including complex many-body processes such as electron correlation in heavy-fermion metals.[1] The investigation of the electron dynamics in metals is often challenging due to the high relaxation rates associated with the intrinsic large carrier densities in metals, as already realized by Drude.[2] The few-femtosecond electronic dephasing, in particular, is one of the fastest processes, governing the initial interaction of an optical field with the metal. This process also rules the temporal evolution of the coherent charge density oscillations of quasi-free conduction electrons in the form of both localized and propagating surface plasmon polaritons (SPPs). The dephasing time T_2 relates to the local field enhancement f of metal nanoparticles as $f \propto T_2$, thus affecting the functionality of optical antennas and plasmonic nanostructures for sensing applications or the degrees of freedom for coherent control on the nanoscale.[3,4] The study of the ultrafast dephasing dynamics provides insight into the validity and limitations of the Fermi-liquid theory and the Drude model to describe conduction electrons in metals.[1]

Many time-domain,[5−12] frequency-domain,[13−15] and most notably spatiotemporal measurements[16] on different Au and Ag nanostructures have established dephasing times ranging from sub-10 fs to several tens of femtoseconds. These time scales are at the limits of current optical pulse generation and characterization schemes in the visible to near-IR spectral range. Therefore, signal analysis and accurate assignment of an intrinsic dephasing time are challenging and typically rely on several ad hoc assumptions,[17] for example, a transform-limited spectral phase of the driving laser pulse, a constant relative signal phase with respect to the nonresonant background, and a Lorentzian line shape from a harmonic oscillator approximation. The presence of ensemble inhomogeneities also complicates the signal analysis. The widely used approach of incoherent dark-field scattering is generally imprecise due to the lack of phase information,

* To whom correspondence should be addressed, raschke@chem.washington.edu.

[⊥] These authors contributed equally to this work.

[#] Present address: Femtolasers Productions GmbH, Vienna, Austria.

Received for review: 03/28/2010
Published on Web: 06/02/2010

except for the characterization of simple resonances, and is not suitable for the analysis of the more complex plasmon dynamics in coupled nanostructures. Also, as a frequency domain measurement, the fast time scales are encoded in details of the spectral wings where the signal level is low and sensitive to background and noise.

Here, we demonstrate the determination of the optical response function and plasmon decoherence of a single metal nanostructure with both amplitude and phase information without specific model assumptions about the nature of the resonance. This is achieved from analysis of the spectrogram of simultaneous time- and frequency-domain measurements of the collinear interferometric second-order autocorrelation of the SPP response. The approach is conceptually similar to frequency-resolved optical gating (FROG) as used for laser pulse characterization.[18]

We study the SPP excitation by symmetry selective second-harmonic (SH) Rayleigh scattering of a radially symmetric nanoscopic conical tip as an individual nanostructure. The real time dynamics of the plasmon dephasing is observed, with a time scale of 18 ± 5 fs. This is in agreement with the longest dephasing times as expected for a nominally homogeneous single particle SPP response in the Rayleigh limit given by the Drude-type dielectric response in the near-IR with the local bulk approximation. Details in phase behavior and its deviation from harmonic oscillator behavior may reflect the effects of intrinsic structural inhomogeneities on the underlying electron ensemble.

Understanding the plasmon response of conical tips chosen as a model system for this investigation is of great interest for tip-enhanced and tip-scattering scanning near-field optical microscopy,[19] adiabatic plasmonic nanofocusing,[20,21] nonlinear wave-mixing,[22] ultrafast local probe photoemission,[23,24] and for new concepts of atom trapping by plasmonic fields with nanotips.[25] The radially symmetric free-standing tips, with the symmetry broken in the axial direction (∞mm symmetry) allow for a pure SH dipole signal under transverse sagittal $\boldsymbol{p}_{in}\boldsymbol{p}_{out}$ polarized pump excitation and SH detection (Figure 1b). This experimental configuration is unique, with all nonlocal higher-order contributions to the SH-polarization from field-gradient and the retardation effects oriented parallel to the incident $\boldsymbol{k}$-vector,[26,27] and thus not observable in this geometry. This allows for selective and background free probing of the isolated axial SPP mode.[28] The resulting source of the SHG emission is the induced local second-order surface polarization density at the apex $\boldsymbol{P}^{(2)}(2\omega) = \varepsilon_0\chi_s^{(2)}L(2\omega)L(\omega)L(\omega):\boldsymbol{E}(\omega)\boldsymbol{E}(\omega)$, with the surface nonlinear susceptibility tensor $\chi_s^{(2)}$ (dominated by component $\chi_{s,\perp\perp\perp}^{(2)}$), and the local-field factors $L(\omega)$ and $L(2\omega)$ for the pump fundamental and generated SH fields $\boldsymbol{E}(\omega)$ and $\boldsymbol{E}(2\omega)$, respectively. For polycrystalline gold surfaces typical values[29] for $\chi_{s,\perp\perp\perp}^{(2)}$ are $\sim 1 \times 10^{-19}$ m^2/V. For the tips used in the experiment, we have previously established a SHG local-field enhancement[26] of order 5×10^3 to 4×10^4 for a one-photon resonant plasmon response at the fundamental laser frequency, corresponding to $L(\omega) \sim 10-20$, consistent with theoretical values.[30]

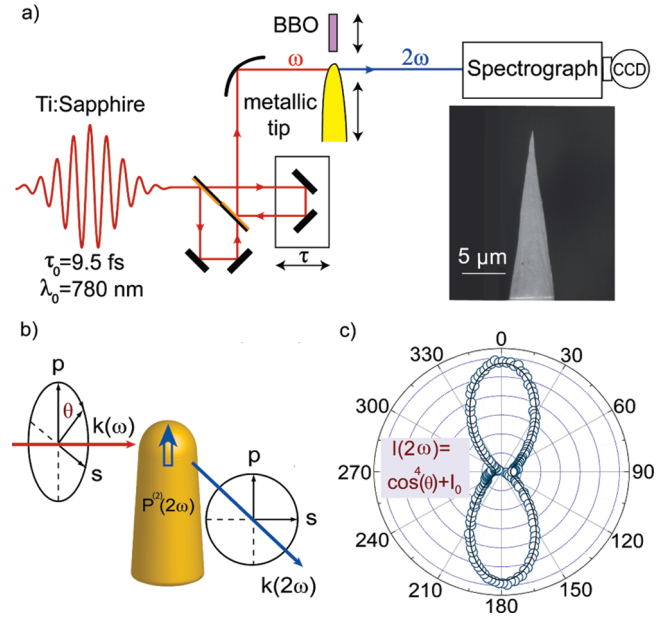

FIGURE 1. (a) Schematic of spectrally resolved interferometric autocorrelation setup for measurement of the SH Rayleigh scattering of the plasmonic tip. The recombined collinear pulses are focused by parabolic mirror and used to study the pump pulse transient or the full plasmonic response function. (b) Scattering geometry with 90° sagittal detection of scattered SHG emission from the tip apex. (c) SHG polarization anisotropy reflecting the broken axial symmetry of the tip.

In using second-order perturbation theory, we then treat the SH-emission as the second-harmonic term of the conventional series expansion of the nonlinear optical polarization,[31] with the fundamental term being the linear polarization $\tilde{P}(t)$ that reflects the response function of the excited plasmon. (Tilde represents a complex-valued property.)

Experimental Section. Gold tips are etched electrochemically with regular shape and apex radius down to ~10 nm as described previously.[32] They are selected for an axial plasmon resonance near the fundamental photon energy of ~1.5 eV,[28] as dictated largely by cone angle, with typical values of 10−20°.

Figure 1a shows the schematic of the second-harmonic two-pulse interferometric autocorrelation setup for the coherent pump−probe experiments, with a dispersion-balanced Michelson interferometer using a 1 mm thick, segmented dielectric beam splitter. Pump−probe delay control employs a linearized and calibrated piezo-controlled translation stage exhibiting ≲0.05 fs root mean square drift and jitter over typical 30 min measurement times. This collinear interferometric implementation, by avoiding crossing wavefront, preserves the full time resolution, provides an internal reference for the delay, and allows for tight focusing by high numerical aperture objectives, which is advantageous for the study of individual nanostructures. In addition, the modula-

DOI: 10.1021/nl101090s | Nano Lett. 2010, 10, 2519–2524

tion intensity of the interference fringes serves as a guide for the optimal alignment of the interferometer.

Broadband Ti:sapphire oscillator pulses (Femtolasers Inc., 80 MHz repetition rate, center wavelength ~780 nm, pulse duration ~10 fs) are used with dispersion precompensation to ensure minimum pulse duration at the Au tip. The tip is mounted interchangeably with a 50 μm thin β- BaB_2O_4 (BBO) crystal. The recombined collinear pulses are focused by means of a 90° off-axis parabolic mirror (focal length 50.8 mm), resulting in a ~20 μm focus diameter, with 100 mW incident power, corresponding to a peak intensity of ~30 GW/cm^2, which is below the onset of higher-order continuum generation.

The tip-scattered SHG emission from the apex is collected at 90° with respect to the incident $\boldsymbol{k}$-vector as shown in Figure 1b), spectrally filtered by a dichroic filter, and detected by a spectrometer with cryogenic CCD camera. Figure 1c shows the polarization anisotropy of the tip SH response detected parallel to the tip axis ($\boldsymbol{p}_{out}$). The solid line corresponds to a normalized fit $I(2\omega) = \cos^4\theta + I_0$ with a residual isotropic term $I_0 = 0.07$ for $\mathbf{s}_{in}\boldsymbol{p}_{out}$ due to deviations from an ideal radial tip symmetry and finite detection angle.

In general, an optical response function $\tilde{R}(t)$ describes the interaction of a stimulating optical field $\tilde{E}(t)$ with the material resulting in the induced optical polarization

$$\tilde{P}(t) = \int \tilde{R}(t - t')\tilde{E}(t')\,dt'$$

Amplitude and phase of the temporal evolution of $\tilde{R}(t)$ can be determined directly by electro-optic sampling or different interferometric homodyne or heterodyne measurement techniques of $\tilde{P}(t)$, provided that decoherence is on time scales longer than the pump and probe transients.[33,34]

For pulse durations and system responses of comparable time scales, the exact reconstruction of the response function is possible by deconvolution from autocorrelation and cross-correlation measurements, provided that the amplitude and phase of pump and probe transients are known. Otherwise, spectrally integrated detection is not sufficient for its unambiguous determination.[18]

In the following, we discuss the reconstruction of amplitude and phase of the underlying system response, and thus its complete characterization, from measurement of the spectrogram of the correlation function.[35] We first use interferometric frequency-resolved optical gating (IFROG)[36−38] to measure

$$I_{IFROG}(2\omega, \tau) \propto \left| \int_{-\infty}^{\infty} (\tilde{X}(t) + \tilde{X}(t - \tau))^2 \exp(-i\omega t)\,dt \right|^2$$

with time delay τ and frequency ω. For a nonlinear medium with nearly instantaneous response far from resonance, e.g., BBO, the field transient $\tilde{X}(t)$ corresponds to the electric field $\tilde{E}(t)$ of the laser pulse. Apart from trivial ambiguities, such as time reversal, the IFROG trace contains all necessary information to unambiguously determine $\tilde{X}(t)$. IFROG in particular offers two independent ways to reconstruct $\tilde{X}(t)$ from the DC as well as the carrier frequency ω_0 modulated part.[38] Here, we use the DC part for retrieval of $\tilde{X}(t)$ as separated by Fourier filtering and processed by a standard FROG retrieval algorithm[18,38] (FROG3, Femtosoft[39]). Subsequently, we measure the IFROG trace of the plasmonic nanostructure as a resonant medium with its finite response time, thus obtaining the induced polarization transient in response to the driving laser pulse, i.e., $\tilde{X}(t) = \tilde{P}(t)$. From $\tilde{E}(t)$ and $\tilde{P}(t)$, standard deconvolution yields the intrinsic SPP response function $\tilde{R}(t)$.

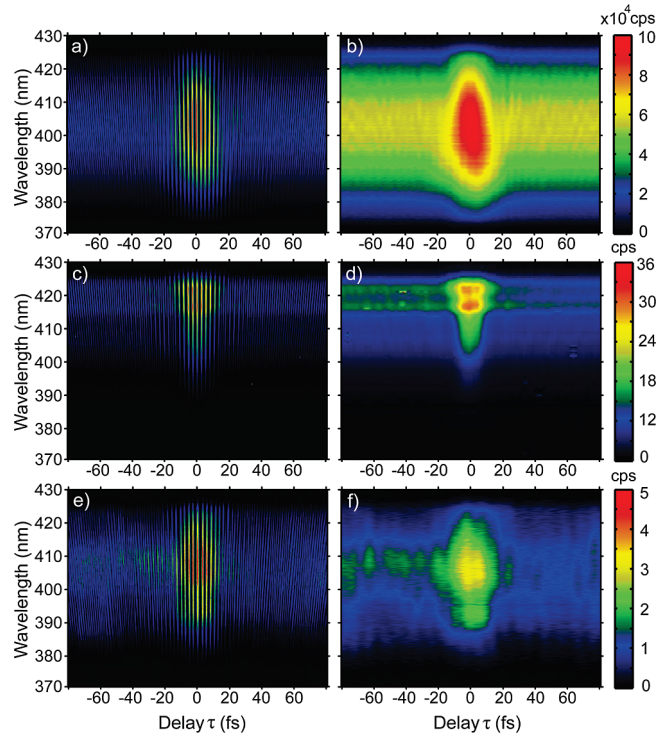

FIGURE 2. Spectrogram of interferometric second-harmonic autocorrelation measurement of BBO (a), plasmon resonant Au tip (c), and off-resonant tip (e). Corresponding Fourier filtered data showing the DC component (b, d, and f).

Results. Figure 2 shows the experimental IFROG trace of BBO (a) in comparison with the corresponding results for a plasmonic tip (c). Measurement of a tip without a plasmon resonance in the accessible spectral range serves as a control experiment (e) with the weak SHG response arising from intraband contributions and nonresonant excitation of conduction electrons. The signal is acquired for ±250 fs (central ±80 fs shown in graph) in 0.15 fs delay steps with 20 s acquisition time per step.

The corresponding DC parts extracted from the IFROG traces via Fourier filtering are shown in panels b, d, and f of Figure 2. The temporally broadened and spectrally narrow response (c and d) is a manifestation of the finite response time of the plasmon excitation. The weak tip signal (e and f) resembles that of the instantaneous BBO response in

DOI: 10.1021/nl101090s | Nano Lett. 2010, 10, 2519--2524

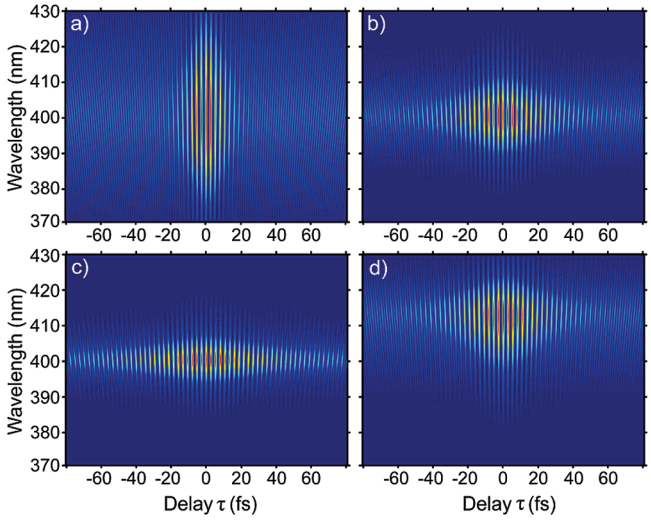

FIGURE 3. Model calculations of typical spectrograms for sech^2 pump pulse (a) of flat spectral phase ($\tau_0 = 9.5$ fs pulse duration); plasmonic response for a damped harmonic oscillator with dephasing time T_2 of 20 fs (b) and 40 fs (c); plasmon response with $T_2 = 20$ fs and offset resonance frequency $\omega_{pl} \neq \omega_0$ (d).

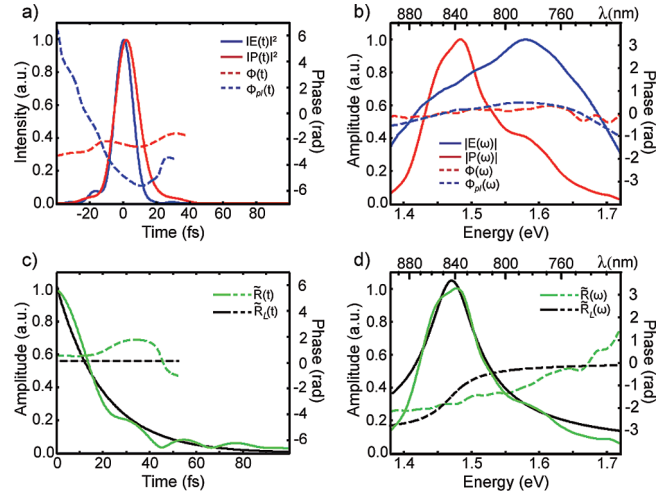

FIGURE 4. Phase (dashed) and intensity (solid line) of $\tilde{E}(t)$ (blue) and $\tilde{P}(t)$ (red) derived from data shown in panels b and d of Figure 2 for pump pulse and plasmon polarization (a) and corresponding Fourier transforms $\tilde{E}(\omega)$ and $\tilde{P}_{pl}(\omega)$ in frequency domain (b). Response function $\tilde{R}(\omega)$ (d) and $\tilde{R}(t)$ (c) (green) from deconvolution of results from (b), in comparison to damped harmonic oscillator model $\tilde{R}_L(\omega)$ (d) with time constant and corresponding Fourier transform $\tilde{R}_L(t)$ (c) (black).

spectral and temporal characteristics as is expected for off-resonance excitation.

Illustrating the effect of a finite response function on the time-frequency spectrogram, Figure 3 shows the results of model calculations. The simulation for BBO as a nonlinear medium is shown in Figure 3a for a laser pulse with flat spectral phase, described by

$$\tilde{E}_{sim}(t) = E_0 \,\mathrm{sech}(1.763t/\tau_0)\exp(i\omega_0 t)$$

with full width at half-maximum $\tau_0 = 9.5$ fs for the intensity profile and carrier frequency ω_0 corresponding to 800 nm center wavelength. We describe the SPP with damped harmonic oscillator response function

$$\tilde{R}_{sim}(t) = A\exp(i\omega_{pl}t - \gamma t/2)$$

where resonance frequency is ω_{pl}, line width is $\gamma = 2/T_2$, and effective oscillator strength is A. The resulting SH spectrograms for $\omega_{pl} = \omega_0$ and $T_2 = 20$ fs (b) and 40 fs (c), respectively, are characterized by corresponding spectral narrowing and temporal broadening. For a plasmon resonance with $\omega_{pl} \neq \omega_0$, shifted by 40 nm with $T_2 = 20$ fs as seen in Figure 3d, the spectrogram becomes distinctly asymmetric due to the finite bandwidth of the laser pulse.

Spectrograms acquired for the same plasmonic tip are in general reproducible yet are often found to be slightly asymmetric. This could be attributed to sample drift or possibly some tip degradation when exposed to the intense laser field. From data analysis of the original spectrogram, and symmetrized spectrograms considering either negative or positive delays, the robustness of the $\tilde{P}(t)$ retrieval can be tested, with corresponding FROG errors of 0.0099 for the original, 0.007 for the negative delay symmetrized, and 0.0067 for positive delay symmetrized spectrograms on a 512 point grid. This allows for the determination of the procedural error in the deconvolution, yielding the uncertainty of the dephasing time we report. While these FROG errors are larger compared to values typical for FROG analysis used for laser pulse characterization, this is due to the weak SHG signal from probing just an individual nanostructure.

Figure 4a shows the resulting intensity $|\tilde{E}(t)|^2$ and phase $\Phi(t)$ of the laser pulse

$$\tilde{E}(t) = E(t)\exp(i\Phi(t))$$

(blue) and intensity $|\tilde{P}_{pl}(t)|^2$ and phase $\Phi_{pl}(t)$, of the plasmon polarization

$$\tilde{P}_{pl}(t) = P(t)\exp(i\Phi_{pl}(t))$$

(red). The corresponding Fourier transforms

$$\tilde{E}(\omega) = \int \tilde{E}(t)\exp(i\omega t)\,dt$$

and

$$\tilde{P}_{pl}(\omega) = \int \tilde{P}_{pl}(t)\exp(i\omega t)\,dt$$

are displayed in Figure 4b). The finite plasmon dephasing temporally extends the polarization response $\tilde{P}_{pl}(t)$ and leads to the correspondingly narrower spectrum $|\tilde{P}_{pl}(\omega)|$ in comparison to the input field. With $\tilde{P}_{pl}(\omega) = \tilde{E}(\omega)\tilde{R}(\omega)$, the response function $\tilde{R}(\omega)$ is obtained from $\tilde{P}_{pl}(\omega)$ and $\tilde{E}(\omega)$ and is shown in Figure 4d) (green). The ambiguity with respect to the sign of the phase is resolved by the fact that all combinations other than these results shown lead to the decay behavior of response function.

Figure 4d shows the result for a numerical fit assuming a single Lorentzian (black) of $\tilde{R}_L(\omega) = A/(\omega - \omega_{pl} + i\gamma/2)$ with center frequency $\hbar\omega_{pl} = 1.47$ eV and $\Gamma = \hbar\gamma = 65$ meV.

DOI: 10.1021/nl101090s | Nano Lett. 2010, 10, 2519–2524

Using the same treatment as in incoherent Rayleigh scattering data analysis, this corresponds to a tip plasmon dephasing time of $T_2 = 20 \pm 5$ fs (with $\Gamma T_2 = 2\hbar$ relating spectral linewidth and dephasing time). More precisely, with the availability of the spectral phase information the Fourier transform provides the corresponding time trace of the plasmon response function $\tilde{R}(t)$ as shown in Figure 4c. Here, we can directly deduce the corresponding dephasing time of $T_2 \sim 18 \pm 5$ fs from the $1/e$ value of maximal amplitude. Although similar within the experimental uncertainty of ± 5 fs with respect to the corresponding value derived from the Lorentzian line width analysis, this deviation reflects the methodological differences of the two approaches as discussed below.

Discussion. With a tip radius on the order of 10−20 nm and the localized SHG response originating from the near-apex region only where the axial symmetry is broken, the tip emission can be treated as a point-dipole in the Rayleigh approximation. This conclusion is validated also from comparison of the experimental results for T_2 with the value estimated from calculating the resonant polarizability for spheroidal particles in the quasi-static limit. Corresponding dephasing times range between 18 and 22 fs for resonant energies between 1.0 and 1.7 eV, in agreement with the experimentally obtained value. Our dephasing time thus corresponds to the low-energy limit and energy-independent damping interpreted in the Drude−Sommerfeld model corresponding to the effective electon scattering rate of ≃9 fs with $T_1 = T_2/2$,[15] dominated by electron−phonon and electron−electron scattering.[40]

Although the SHG photon energy of ∼3 eV leads to interband excitation, due to much shorter dephasing times associated with the d to sp band transition in gold,[41,42] the measured response function can be attributed to the one-photon resonant plasmon excitation. Our dephasing times observed for a plasmon resonance near 1.5 eV, i.e., well below the onset of the interband excitation, can thus be interpreted as the response from the conduction electrons near the Fermi level.

In frequency domain dark field scattering,[15] the time domain dephasing time constant is obtained via the line width and relaxation rate correspondence assuming a Lorentzian spectral shape. To be accurate, this approach requires the plasmonic response to be in good agreement with a single damped harmonic oscillator, further complicated by the fact that the information about the fast dynamics is determined by the broad spectral wings. In addition, this indirectly corresponds to the assumption of a purely homogeneous line width.

Although, our results for the dephasing time compare favorably with results obtained from dark-field scattering experiments of metal nanoparticles with high aspect ratio,[15] with $T_2 \sim 18$ fs for resonance energies of 1.5−1.7 eV, the meaningful use of dark-field scattering is limited to plasmonic nanostructures with simple resonance behavior. In our approach demonstrated here of response function reconstruction, and related to the availability of the phase information as required for the accurate Fourier transform between frequency and time domain, the dephasing time is directly obtained without any model assumption.

The phase behavior observed and the difference between direct read out and Lorentzian line width analysis suggest that the SPP response is inhomogeneously broadened. Inhomogeneities can result from an ensemble of nonidentical particles or, as in the case of an individual nanostructure, structural imperfections within the single plasmonic emitter itself. In addition, despite the collective and coherent SPP excitation, the driven conduction electrons correspond to an inhomogeneous ensemble with different electron scattering pathways including electron-defect and electron−phonon scattering and its temperature dependence. The resulting superposition can result in a flatter than expected phase behavior in the frequency domain and, consequently a slightly shorter dephasing time compared to the line width analysis in the frequency domain. Note that with the dephasing time of 18 fs measured being at the upper limit as described by the bulk dielectric response and the Drude model, radiative damping and contributions from surface scattering and higher order nonlocal effects can be neglected.

In summary, we have integrated the well-established FROG pulse characterization technique into a spectroscopic experiment to provide the complex-valued optical response function of a plasmonic nanostructure. Since the laser pulse is explicitly considered with its full amplitude and phase behavior, the method is generally robust with respect to details of the optical transient of the driving laser pulse. With this method, we have been able to look beyond the ad hoc assumption of a damped harmonic oscillator model. In addition, the deconvolution-based approach can provide dynamic information on time scales faster than the laser pulse duration, in principle only limited by the available signal-to-noise ratio, and is generally applicable for analysis of complex plasmon dynamics of waveguides and coupled nanostructures with multiple resonances and complex phase behavior. It can readily be extended by XFROG[43,44] allowing for the isolation of the effect of the nonresonant background for more precise phase information and to remove the time direction ambuigity[45] of the FROG algorithm. The method is related to similar experiments using the linear technique of spectral interferometry[46] and yet provides a higher contrast due to the lower background of the nonlinear response. Further development of this technique for better amplitude and phase retrieval may enable access to valuable information concerning fundamental intrinsic anharmonicities in the plasmonic response, discern the role of retardation induced phase changes, may further allow for a distinction between homogeneous and inhomogeneous effects, and reveal details of the near-field coupling in complex nanostructures.

DOI: 10.1021/nl101090s | *Nano Lett.* **2010,** *10,* 2519--2524

Acknowledgment. The authors thank Hrvoje Petek, Tony Heinz, Tamar Seideman, Rudolf Bratschitsch for valuable discussions. Funding from the National Science Foundation (NSF Career Grant CHE 0748226) is gratefully acknowledged. Günter Steinmeyer gratefully acknowledges support by the Academy of Finland (project grant 128844).

Note Added after ASAP Publication. A change was made to the last equation associated with Figure 4 in the version of this paper published ASAP June 2, 2010; the correct version published on June 14, 2010.

REFERENCES AND NOTES

(1) Dressel, M.; Scheffler, M. *Ann. Phys.* **2006**, *15*, 535.
(2) Drude, P. *Ann. Phys.* **1900**, *306*, 566.
(3) Aeschlimann, M.; Bauer, M.; Bayer, D.; Brixner, T.; de Abajo, F. J. G.; Pfeiffer, W.; Rohmer, M.; Spindler, C.; Steeb, F. *Nature* **2007**, *446*, 301.
(4) Utikal, T.; Stockman, M.; Heberley, A.; Lippitz, M.; Giessen, H. *Phys. Rev. Lett.* **2010**, *104*, 113903.
(5) Heilweil, E. J.; Hochstrasser, R. M. *J. Chem. Phys.* **1985**, *82*, 4762.
(6) Lamprecht, B.; Leitner, A.; Aussenegg, F. R. *Appl. Phys. B: Laser Opt.* **1999**, *68*, 419.
(7) Liau, Y.-H.; Unterreiner, A.; Chang, Q.; Scherer, N. F. *J. Phys. Chem. B* **2001**, *105*, 2135.
(8) Zentgraf, T.; Christ, A.; Kuhl, J.; Giessen, H. *Phys. Rev. Lett.* **2004**, *93*, 243901.
(9) Mayergoyz, I. D.; Zhang, Z.; Miano, G. *Phys. Rev. Lett.* **2007**, *98*, 147401.
(10) Klein, M. W.; Tritschler, T.; Wegener, M.; Linden, S. *Phys. Rev. B* **2005**, *72*, 115113.
(11) Utikal, T.; Zentgraf, T.; Kuhl, J.; Giessen, H. *Phys. Rev. B* **2007**, *76*, 245107.
(12) Hanke, T.; Krauss, G.; Träutlein, D.; Wild, B.; Bratschitsch, R.; Leitenstorfer, A. *Phys. Rev. Lett.* **2009**, *103*, 257404.
(13) Stietz, F.; Bosbach, J.; Wenzel, T.; Vartanyan, T.; Goldmann, A.; Träger, F. *Phys. Rev. Lett.* **2000**, *84*, 5644.
(14) Hubenthal, F. *Prog. Surf. Sci.* **2007**, *82*, 378.
(15) Sönnichsen, C.; Franzl, T.; Wilk, T.; von Plessen, G.; Feldmann, J.; Wilson, O.; Mulvaney, P. *Phys. Rev. Lett.* **2002**, *88*, No. 077402.
(16) Kubo, A.; Onda, K.; Petek, H.; Sun, Z.; Jung, Y. S.; Kim, H. K. *Nano Lett.* **2005**, *5*, 1123.
(17) Lamprecht, B.; Leitner, A.; Aussenegg, F. R. *Appl. Phys. B: Laser Opt.* **1997**, *64*, 269.
(18) Trebino, R. *Frequency Resolved Optical Gating: The Measurement of Ultrashort Laser Pulses*; Kluwer: Boston, MA, 2002.
(19) Neacsu, C. C.; Dreyer, J.; Behr, N.; Raschke, M. B. *Phys. Rev. B* **2006**, *73*, 193406.
(20) Stockman, M. I. *Phys. Rev. Lett.* **2004**, *93*, 137404.
(21) Neacsu, C. C.; Berweger, S.; Olmon, R. L.; Saraf, L. V.; Ropers, C.; Raschke, M. B. *Nano Lett.* **2010**, *10*, 592.
(22) Bouhelier, A.; Beversluis, M.; Hartschuh, A.; Novotny, L. *Phys. Rev. Lett.* **2003**, *90*, No. 013903.
(23) Stockman, M. I.; Kling, M. F.; Kleineberg, U.; Krausz, F. *Nat. Photonics* **2007**, *1*, 539.
(24) Ropers, C.; Solli, D. R.; Schulz, C. P.; Lienau, C.; Elsaesser, T. *Phys. Rev. Lett.* **2007**, *98*, No. 043907.
(25) Chang, D. E.; Thompson, J. D.; Park, H.; Vuletic, V.; Zibrov, A. S.; Zoller, P.; Lukin, M. D. *Phys. Rev. Lett.* **2009**, *103*, 123004.
(26) Neacsu, C. C.; Reider, G. A.; Raschke, M. B. *Phys. Rev. B* **2005**, *71*, 201402(R).
(27) Dadap, J. I.; Shan, J.; Eisenthal, K. B.; Heinz, T. F. *Phys. Rev. Lett.* **1999**, *83*, 4045.
(28) Neacsu, C. C.; Steudle, G. A.; Raschke, M. B. *Appl. Phys. B: Laser Opt.* **2005**, *80*, 295.
(29) Krause, D.; Teplin, C. W.; Rogers, C. T. *J. Appl. Phys.* **2004**, *96*, 3626.
(30) Behr, N.; Raschke, M. B. *J. Phys. Chem. C* **2008**, *112*, 3766.
(31) Boyd, R. *Nonlinear Optics*; Elsevier: Amsterdam, 2008.
(32) Neacsu, C. C.; Berweger, S.; Raschke, M. B. *Nanobiotechnology* **2009**, *3*, 172.
(33) Kampfrath, T.; Beggs, D. M.; Krauss, T. F.; Kuipers, L. K. *Opt. Lett.* **2009**, *34*, 3418.
(34) Weiner, A. M. *Ultrafast Optics*; Wiley: Hoboken, NJ, 2009.
(35) *Image recovery: Theory and application*; Stark, H., Ed.; Academic Press: Orlando, FL, 1987.
(36) Amat-Roldán, I.; Cormack, I.; Loza-Alvarez, P.; Gualda, E.; Artigas, D. *Opt. Express* **2004**, *12*, 1169.
(37) Stibenz, G.; Steinmeyer, G. *IEEE J. Sel. Top. Quantum Electron.* **2006**, *12*, 286.
(38) Stibenz, G.; Steinmeyer, G. *Opt. Express* **2005**, *13*, 2617.
(39) DeLong, K. W.; Fittinghoff, D. N.; Trebino, R.; Kohler, B.; Wilson, K. *Opt. Lett.* **1994**, *19*, 2152.
(40) Liu, M.; Pelton, M.; Guyot-Sionnest, P. *Phys. Rev. B* **2009**, *79*, No. 035418.
(41) Petek, H.; Ogawa, S. *Prog. Surf. Sci.* **1997**, *56*, 239.
(42) Ogawa, S.; Nagano, H.; Petek, H.; Heberle, A. P. *Phys. Rev. Lett.* **1997**, *78*, 1339.
(43) Linden, S.; Giessen, H.; Kuhl, J. *Phys. Status Solidi B* **1998**, *206*, 119.
(44) Xu, X. G.; Konorov, S. O.; Zhdanovich, S.; Hepburn, J. W.; Milner, V. *J. Chem. Phys.* **2007**, *126*, No. 091102.
(45) Zeek, E.; Shreenath, A. P.; O'Shea, P.; Kimmel, M.; Trebino, R. *Appl. Phys. B: Laser Opt.* **2002**, *74*, S265.
(46) Ropers, C.; Park, D. J.; Stibenz, G.; Steinmeyer, G.; Kim, J.; Kim, D. S.; Lienau, C. *Phys. Rev. Lett.* **2005**, *94*, 113901.

DOI: 10.1021/nl101090s | *Nano Lett.* **2010,** *10,* 2519--2524